High Pressure–High Temperature Polymorphism and Decomposition of Pentaerythritol Tetranitrate (PETN)

ARTICLE *in* THE JOURNAL OF PHYSICAL CHEMISTRY A · JUNE 2013

Impact Factor: 2.69 · DOI: 10.1021/jp404283a · Source: PubMed

THE JOURNAL OF PHYSICAL CHEMISTRY A

Article

pubs.acs.org/JPCA

High Pressure–High Temperature Polymorphism and Decomposition of Pentaerythritol Tetranitrate (PETN)

Zbigniew A. Dreger* and Yogendra M. Gupta

Institute for Shock Physics and Department of Physics and Astronomy, Washington State University, Pullman, Washington 99164-2816, United States

ABSTRACT: To elucidate the behavior of PETN at thermo-mechanical conditions relevant for shock initiation, Raman spectroscopy, and optical imaging were used to examine its static high pressure and high temperature (HP–HT) response. Experiments were performed on single crystals in a heated diamond anvil cell at pressures to 14 GPa and temperatures ranging from room temperatures to 550 K. Regarding the pressure-induced PETN-I transition to PETN-III at room temperature, our results show that nonhydrostaticity plays an important role in driving this transition. Furthermore, we found that PETN-III transforms to PETN-IV at high temperatures, and this transformation can involve lowering of molecular symmetry from C_2 to C_1. The HP–HT phase diagram for PETN presented here includes the melting/decomposition curve and boundaries between three PETN phases: PETN-I, PETN-III, and PETN-IV. The relevance of static compression results for shock initiation of PETN is discussed.

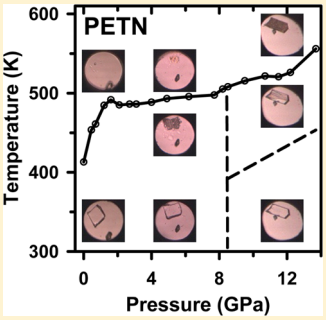

1. INTRODUCTION

Pentaerythritol tetranitrate (PETN; $C(CH_2ONO_2)_4$), the nitrate ester of pentaerythritol, is one of the most important crystalline energetic materials, extensively used as an ingredient in many high explosive (HE) formulations. It has attracted considerable scientific attention due to its anisotropic sensitivity to shock wave initiation.[1,2]

A number of studies have been undertaken to understand the observed anisotropic sensitivity.[3−10] In particular, a model was developed that linked the observed anisotropic sensitivity to differences in molecular changes occurring in crystals shocked along different orientations.[6] Specifically, the large sensitivity observed for shocks along the [110] orientation was attributed to shear deformation induced conformational changes induced in PETN molecules. Subsequently, the conformational changes resulted in local polarization and lead to initiation of ionic reactions.

The key elements of the above-indicated model[6] were successively examined in our laboratory, both computationally and experimentally. From shock-induced light emission experiments, it was deduced that the nitronium ion (NO_2^+) can be a decomposition intermediate resulting from the ionic decomposition process,[7] in accordance with the model.[6] Furthermore, propensity of PETN molecules to conformational changes was assessed with semiempirical methods, which indicated that changes in conformation/symmetry can be readily observed through changes in the vibrational spectra.[9] Subsequently, real time, high spectral resolution Raman measurements on shocked PETN revealed new features in the spectra of crystal shocked along the [110] (sensitive) orientation to 6.5 GPa.[8] Analyses of the shock spectra in conjunction with spectra obtained on statically compressed PETN[9] indicated that the new features could be associated with conformational changes in shocked PETN. This conclusion was based on similarities between the shocked and static pressure Raman spectra. However, the latter were obtained at room temperature (RT) and at relatively low pressures (up to ∼5 GPa), at thermo-mechanical conditions different from those that occur under shock compression.

Since shock compression of HE crystals results in both high compression and high temperature, static high pressure (HP) data at high temperatures (HT) rather than at RT are needed for a more meaningful comparison of conformational changes in PETN under the two sets of loading conditions. To address this need, we examined the PETN response under static compression over the range of pressures and temperatures relevant to shock initiation. As recently demonstrated for RDX (cyclotrimethylene trinitramine) crystals, static HP–HT data can provide important insight into HE reactive behavior, which is often difficult to achieve directly from shock experiments.[11−14]

Next, we briefly summarize previous PETN studies at static high pressures. The structure of PETN at ambient pressure is well established.[15−17] At room temperature, it is tetragonal ($P\bar{4}2_1c$ space group) with four molecules of S_4 symmetry per unit cell as shown in Figure 1. It was also reported that this structure (PETN-I) can transform to PETN-II just before melting (∼414 K) to assume the *Pcnb* space group.[17]

In contrast to ambient pressure, PETN response under static high pressures is not as well established.[9,18−22] There are no HP–HT data, and reports on the RT high pressure response are conflicting. We first reported on changes in Raman spectra above ∼5 GPa, which were attributed to the molecular symmetry change from S_4 to C_2.[9] Also, the transition of PETN-I to PETN-III having an orthorhombic structure and a

Received: April 30, 2013
Revised: May 25, 2013
Published: June 3, 2013

dx.doi.org/10.1021/jp404283a | *J. Phys. Chem. A* 2013, 117, 5306−5313

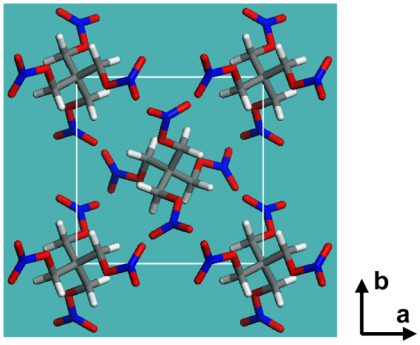

Figure 1. Projection of PETN crystal structure on the *ab* plane. Molecules are represented using a stick model. Legend: carbon, gray; oxygen, red; nitrogen, blue; hydrogen, white.

$P2_12_12$ space group was proposed. Subsequently, several studies reported changes in Raman and IR spectra, and X-ray diffraction patterns under high pressures.[18−22] However, the onset of spectral changes observed in those later studies ranged from ∼6 to 9.5 GPa. Furthermore, conclusions regarding the possible high pressure structure were not consistent between different reports. For example, from powder X-ray diffraction measurements and first-principle calculations, Tschauner et al.[22] deduced that PETN-III could assume an orthorhombic structure with the space group of $P2_12_12$, but with the same molecular symmetry as in PETN-I. In contrast, on the basis of Raman measurements on powder and single grain samples, Ciezak et al.[21] proposed that PETN-III maintains the same crystal structure as PETN-I but with molecules assuming the D_2 symmetry.

This brief summary above indicates that PETN response under static compression depends strongly on experimental conditions, including the quality and state of samples and pressure. Therefore, to avoid inconsistencies due to random sample morphology, grain interactions, and uncertain compression conditions, the experiments reported here were performed using good quality single crystals and under controlled pressure loading.

The main objective of this work was to examine the structural and reactive response of PETN crystals over a broad range of pressures and temperatures to provide further insight into the PETN shock wave initiation. We used Raman spectroscopy along with optical imaging to distinguish between different PETN phases. The specific issues of interest were (i) to re-examine the structure stability at high pressure and room temperature with respect to the reported phase change; (ii) to determine the HP-HT response, including the phase diagram and the melting/decomposition curve; and (iii) to relate the static HP−HT results to shock wave initiation of PETN.

The remainder of this article is organized as follows. Experimental procedures are described briefly in the next section. Sections 3 and 4 present experimental data and discussions regarding the objectives listed above. The main findings of this work are summarized in Section 5.

2. EXPERIMENTAL METHODS

Small single crystals of PETN were grown from an acetone solution using PETN polycrystals provided by Dr. D. E. Hooks of Los Alamos National Laboratory. Typical crystals had approximately rectangle shape and a thickness of about 30 μm. The crystals used in our experiments were grown from the same batch and were carefully selected to ensure comparable size and quality.

High pressures were produced using a modified Merrill−Bassett type diamond anvil cell (DAC). A spring-steel gasket, preindented to 0.06−0.08 mm with a 0.125 or 0.200 mm hole drilled in the indentation, was used as a sample compartment. A PETN single crystal and a ruby chip were loaded into the sample compartment, and cryogenically loaded argon was used as an inert pressure transmitting medium. The ruby fluorescence method utilizing R-line shifts was used to monitor pressure. The precision of our pressure measurements was estimated to be ∼0.05 GPa.

Temperature of the DAC was varied using a resistive heater wrapped around the cell. The sample temperature was monitored using iron−constantan thermocouples. The accuracy of the temperature measurements in our experiments was estimated to be ±2 K and was determined as a standard deviation from several controlled experiments.

A micro-Raman system (T64000, JY-Horiba) equipped with a microscope (Olympus BX-40) was used to provide the spectra and images of PETN at various pressures and temperatures. The 532 nm line from a cw diode-pumped solid-state (DPSS) laser (Verdi-Coherent) was employed for Raman excitation. The incident power on the sample did not exceed 50 mW to avoid any photochemical effects. Furthermore, the laser spot size was adjusted to acquire signal from most of the sample and was typically about 50 μm in diameter. Further details regarding our micro-Raman and ruby fluorescence measurement techniques can be found elsewhere.[11−14]

3. RESULTS AND DISCUSSION

3.1. High Pressure−Room Temperature Response: PETN-I to PETN-III Transition. In Figure 2, we show the Raman spectra of PETN at several pressures, using argon as pressure transmitting medium. Our data show that pressure-induced changes up to ∼8.5 GPa consist primarily of frequency shifts. However, above this pressure new features gradually develop in the spectra and are completed by 9.2 GPa. In the frequency range below 1000 cm^{-1} (Figure 2a), the changes include (i) broadening and disappearance of modes assigned to external vibrations, (ii) replacement of the strong mode (CCC deformation + ONO_2 rock)[23] initially located at 624 cm^{-1} by a group of at least four peaks, and (iii) development of strong peaks on the low frequency side of the mode (O−N stretching + CC stretching)[23] initially located at 873 cm^{-1}. Furthermore, as seen in Figure 2b, the CH stretching modes split into doublets. Also, two other observations are noteworthy. First, despite significant changes in the spectra, the sample seemed to be macroscopically unaltered (see images in Figure 2b). Second, the changes in the spectra were reversible after a slow release of pressure; despite this reversibility, the sample often showed cracks. All of these findings are inconsistent with that reported.[21]

In Figure 3, we demonstrate the effect of nonhydrostaticity on the changes in Raman spectra. For this, we have compared spectra obtained in argon with those in glycerol, at transition pressures obtained for each media; also these spectra are compared with the spectra calculated for the C_2 molecular conformer of PETN.[9] It is clear that spectral changes occur at very different pressures in the two media: at 9.2 and 5.3 GPa, respectively, in argon and in glycerol. Despite this large difference in pressure, the spectra shapes are quite similar. Both

dx.doi.org/10.1021/jp404283a | J. Phys. Chem. A 2013, 117, 5306−5313

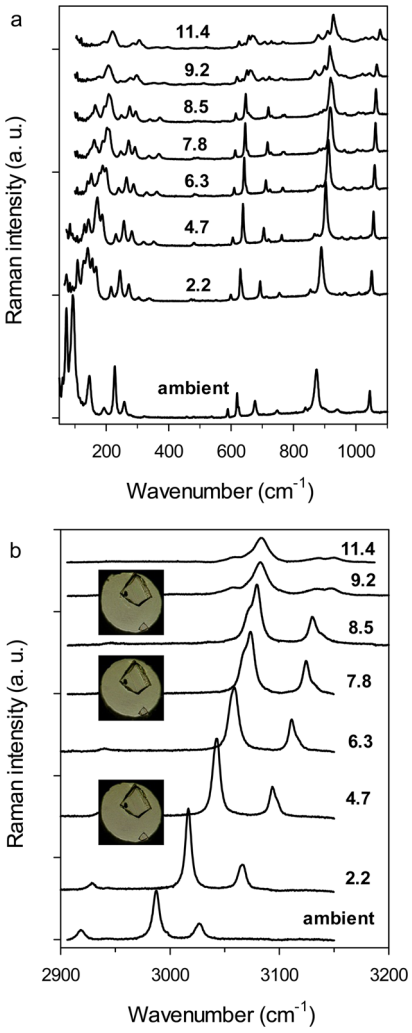

Figure 2. Raman spectra of PETN single crystal at several pressures in argon pressure transmitting medium. Top graph presents spectra in the range of external and low frequency modes. Bottom graph presents spectra in the range of CH stretching modes. Also, sample images at several pressures are shown next to the spectra at 4.7, 7.8, and 9.2 GPa. Spectra are offset vertically for clarity. Pressures are given in GPa.

spectra exhibit comparable patterns of peaks either in the range 600−680 cm^{-1}, 5 peaks, or 680−800 cm^{-1}, another 5−6 peaks. Also, in the range of CH stretching vibrations there are clear splitting of two modes in both cases. Qualitative agreement of these results suggests that regardless of the large difference in pressures, PETN undergoes the same transformation.

Furthermore, experimental spectra (Figure 3) are in good agreement with features in the calculated spectra for the C_2 molecular conformer. The approach for calculating the vibrational spectra of PETN molecular conformers was presented in our previous paper;[9] we note that the calculations were performed using a single molecule. Despite this simplification, we demonstrated that this approach provided a good approximation to the experimental spectrum at ambient conditions.[9] The close similarity of the experimental spectra obtained here to the calculated spectra for C_2 molecular conformer further supports our previous proposal[9] of the molecular symmetry change from S_4 to C_2 under high pressure.

To evaluate possible changes in the crystal structure associated with the molecular transition at 9.2 GPa, we examined spectral changes in the low frequency range,

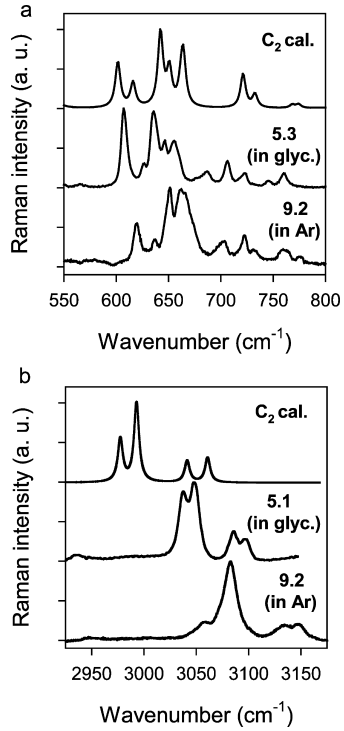

Figure 3. Selected Raman spectra of PETN obtained in argon and glycerol pressure media and calculated spectra for C_2 symmetry of a single PETN molecule. Raman spectrum in the glycerol and the calculated spectra are from ref 9. (a) Spectral region including the CCC deformation modes and (b) spectral region of CH stretching modes. Pressures are given in GPa.

including lattice modes. In Figure 4, we show a close-up view of the Raman spectra in this range. Examination of these

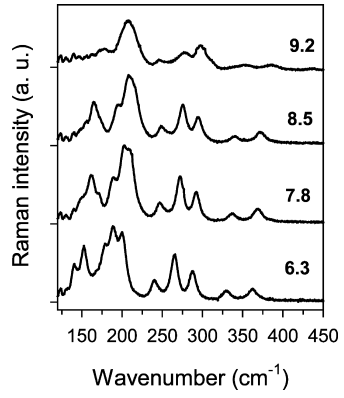

Figure 4. Close-up view of Raman spectra in the low frequency region. Only spectra at pressures close to the phase transition are shown. Pressures are given in GPa.

spectra reveals several new features at 9.2 GPa: (i) broadening of most peaks, likely due to some structure disorder, (ii) shift of the peak located at ∼249 cm^{-1} to lower frequencies, due to mode softening, and (iii) asymmetric broadening, seemingly due to splitting of peaks at ∼275 and 295 cm^{-1}. These results clearly imply changes in the crystal structure in addition to the molecular changes discussed above. An apparent increase in the number of modes can imply a decrease in the crystal symmetry. This finding is consistent with our previous suggestion of the structure changing from tetragonal to orthorhombic.[9] As

dx.doi.org/10.1021/jp404283a | J. Phys. Chem. A 2013, 117, 5306−5313

discussed previously[9] and later confirmed by powder X-ray measurements,[22] the most probable space group for the high pressure phase is $P2_12_12$.

As shown above, the single crystal results presented here are in contrast to results in previous reports.[18−22] Although the present results support our earlier finding and conclusions regarding the PETN phase transformation at high pressures,[9] the pressure onset for this transformation depends on the pressure transmitting media and demonstrates that non-hydrostaticity is an important factor in driving this transition. Furthermore, it appears that several factors, including molecular flexibility, anisotropy in crystal interactions, and crystal deformation can play role in this transition.

3.2. High Pressure−High Temperature Response. Because argon provides a more hydrostatic pressure environment than glycerol,[24] all our HP−HT experiments were performed with argon as a pressure transmitting medium. To determine the PETN phase diagram, we first established the P−T boundary for PETN melting/decomposition and then examined the solid phase behavior in the P−T domain below this boundary.

3.2.1. P−T Upper Bound for Melting/Decomposition. To examine the P−T conditions for PETN melting/decomposition, the crystals were compressed to different pressures and then gradually heated. Raman spectra and optical images were used to monitor structural and chemical changes in the crystal. In particular, changes in the intensity of the Raman peaks and the sample appearance were used to evaluate the upper temperature bound for melting and/or decomposition. All experiments were performed using a heating rate of ∼1 K/min. This rate was selected after examining the effect of different heating rates on the decomposition temperature. Because there was no measurable difference in the observed decomposition temperatures for rates from 1 to 4 K/min, we selected 1 K/min. This value better matched the thermal response of the cell and was also used in previous studies.[13,14]

In Figure 5, we present selected images of crystals compressed to three different pressures (0.7, 3.1, and 10.7 GPa) and heated at the rate ∼1 K/min. These results represent three distinct differences in the PETN response at high temperatures. For pressures below ∼2 GPa, the heated PETN crystal clearly melted. As seen in a series of images obtained at 0.7 GPa, starting at 456 K, the sample gradually disappears in liquid argon. For pressures between 2 and 6 GPa, both melting and decomposition were observed. The results at 3.1 GPa are typical of the interplay between disappearance and darkening of the sample. This process starts at ∼476 K and ultimately leaves decomposed residue by 496 K. For pressures above ∼6 GPa, PETN decomposed instead of melting. It is noteworthy that the sample remained intact after decomposition, see the image at 10.7 GPa and 532 K. Additionally, experiments at pressures above ∼8.5 GPa showed that decomposition was preceded by the formation of parallel lines on the crystal. This feature can be seen in the images obtained at 10.7 GPa. The lines occur initially at the crystal edge at 429 K and then propagate across the crystal as the temperature increases. Although the formation of lines was completed by 476 K, decomposition onset was observed only above 520 K. As shown in the next section, the macroscopic changes to the sample were accompanied by changes in the Raman spectra.

The melting/decomposition results acquired from numerous high pressure experiments are consolidated in Figure 6; the vertical lines denote the temperature range over which the melting/decomposition was observed. The melting or decomposition temperature bounds were estimated from a decrease in the Raman intensity and darkening or disappearing of the sample. The temperature accuracy was estimated to be ±2 K. To guide the eye, the centers of bars are connected by lines. In other words, the resulting curve denotes the temperatures at which half of the sample was decomposed. The results in Figure 6 demonstrate several key features: (i) below 2 GPa, PETN melts, and the melting temperature increases rapidly with pressure; (ii) between 2 and 6 GPa, there is an interplay between melting and decomposition, and the temperature for this process indicates a shallow saddle around ∼3 GPa; and (iii) above 6 GPa, there is only decomposition, and the temperature for this process increases monotonically with pressure.

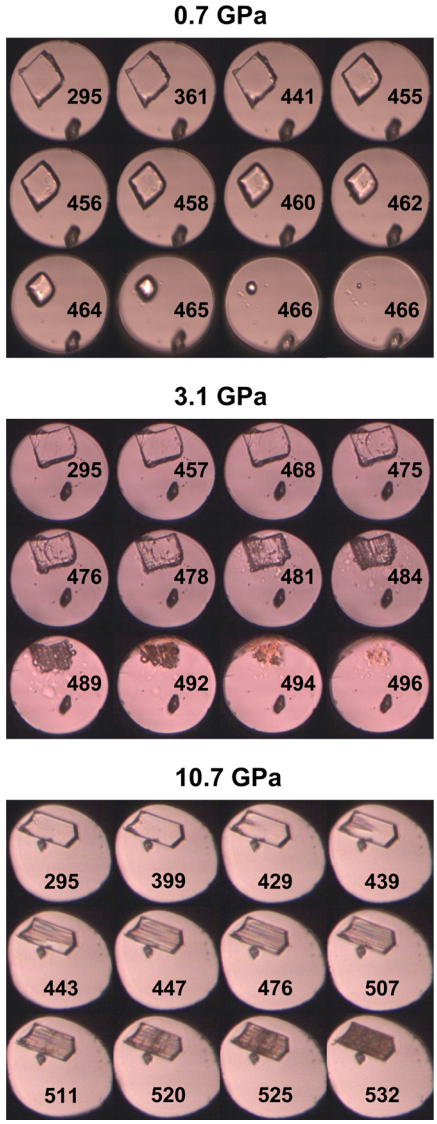

Figure 5. Selected optical images of PETN crystal at (a) 0.7, (b) 3.1, and (c) 10.7 GPa obtained during heating of crystals at a rate of ∼1 K/min. Images represent three characteristic behaviors of samples at HP−HT. At 10.7 GPa, well-distinct lines propagate across the crystal at the selected temperatures. The results obtained at other higher pressures indicate that the origin of lines initiation is not related to the sample location in the cell. The hole in the gasket was ∼0.200 μm. A black spot in each image is a ruby grain. Temperatures are given in Kelvin.

dx.doi.org/10.1021/jp404283a | J. Phys. Chem. A 2013, 117, 5306−5313

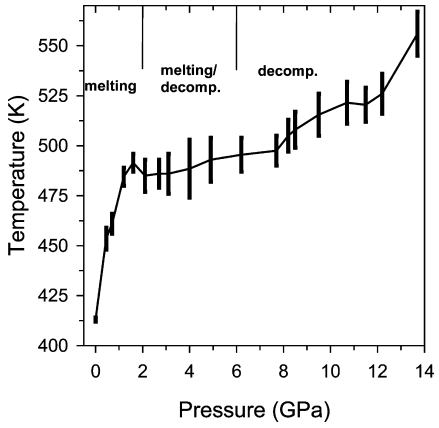

Figure 6. P–T upper bound for PETN melting/decomposition. Vertical bars denote the onset and completion of melting and/or decomposition as determined from Raman spectra and optical images, while heating the sample at a rate of ~1 K/min. The curve connecting the centers of the vertical bars was drawn to guide the eye. The vertical lines at the top of the graph indicate the pressure ranges at which crystal melts, melts/decomposes, and decomposes.

3.2.2. PETN-III to PETN-IV Transition. The solid phase of PETN, below the melting/decomposition curve, was monitored using Raman measurements. In Figure 7, we present a

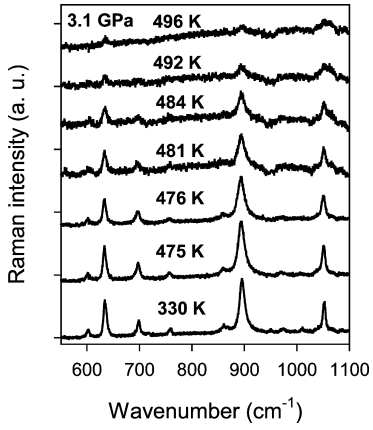

Figure 7. Selected Raman spectra of PETN at 3.1 GPa obtained while heating the sample at a rate of 1 K/min. Signal was acquired for 10 s in each case.

representative example of Raman spectra obtained at several temperatures at a pressure of 3.1 GPa. No apparent changes were observed up to ~475 K, implying that the crystal remained in the same phase at all temperatures. At ~476 K, the intensity of the peaks decreases indicating the onset of decomposition. With further increase of temperature, the Raman peaks quickly deteriorate and ultimately vanish at ~496 K. This behavior was observed for pressures below ~8.5 GPa, suggesting that PETN-I maintains the same phase over the entire temperature range that was examined.

In contrast to PETN-I, the behavior of PETN-III (formed above 8.5 GPa) showed temperature-induced changes in the Raman spectra prior to decomposition. As an example, Raman spectra at 9.2 GPa are presented in Figure 8, where we compare the spectra obtained at several temperatures. Initially, the temperature increase does not affect the spectrum as seen from the similarity between the spectra at 381 K and at room

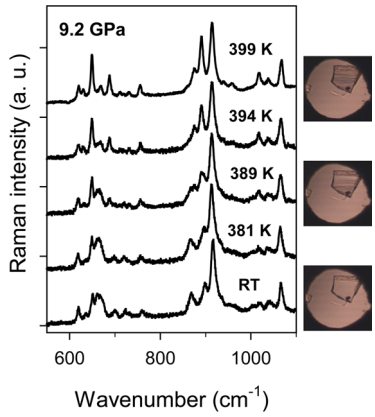

Figure 8. Raman spectra of PETN at 9.2 GPa and several temperatures. Spectrum at 399 K was accumulated for 30 s and the other spectra for 20 s. Images represent changes in the crystals at room temperature (RT) and 389 and 399 K.

temperature (RT). However, further temperature increase gradually transforms the spectra. These spectral changes occur at 389 K, the same temperature when the deformation lines appear on the crystal. Additional temperature increase brings the transformation to completion above 399 K. To identify detailed changes in the high temperature spectra, we compare spectra at 409 K and room temperatures in Figure 9.

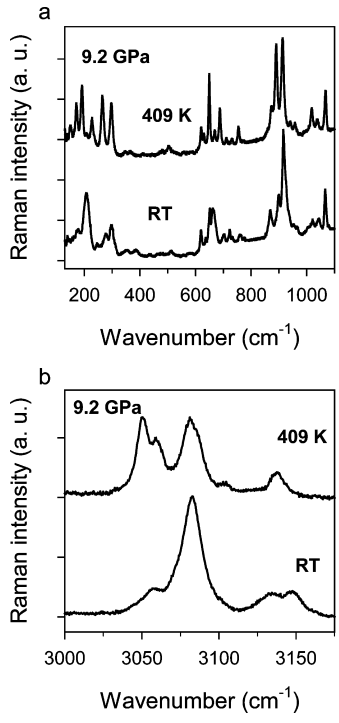

Figure 9. Raman spectra of PETN crystal at 9.2 GPa obtained at RT and 409 K. (a) External and low frequency modes and (b) CH stretching modes.

In the low frequency range below 1000 cm^{-1}, the HT spectrum seems to have a similar number of peaks as the RT spectrum. However, there are also some differences between the two spectra: (i) HT spectrum has narrower and better resolved peaks than the RT spectrum; (ii) relative intensities of several peaks are different in the two spectra; (iii) patterns of the peaks are significantly different below 200 cm^{-1} and between 600 and

dx.doi.org/10.1021/jp404283a | J. Phys. Chem. A 2013, 117, 5306–5313

800 cm^{-1} in the two spectra; and (iv) several peaks (e.g., 687, 711, and 874 cm^{-1}) are shifted to higher frequencies with respect to their positions at RT, opposite to the expected shifts with temperature. In addition, comparison of the spectra in the CH stretching region, shown in Figure 9b, indicates significant differences in the shape of two spectra. The HT spectrum clearly shows a larger number of peaks than the RT spectrum. These differences between the two spectra demonstrate that PETN-III undergoes a transformation to another form, PETN-IV, at high temperatures.

To gain insight into the possible structure of PETN-IV, we compared the HP–HT spectra with selected spectra calculated for different PETN conformers. Though the calculated spectra are for a single molecule,[9] they are helpful in narrowing down the possibilities for the PETN-IV structure. The experimental spectra of PETN-IV (9.2 GPa, 409 K) are compared with the calculated spectra in Figure 10. In the frequency range 600–800 cm^{-1}, we can distinguish nine peaks in the experimental as well as in all calculated spectra. Though the patterns of the peaks are different in each case, the finding of the same number of peaks in experimental and calculated spectra makes it difficult to distinguish structural differences between the PETN-III and PETN-IV. However, useful insight is obtained from comparison of the spectra in the CH stretching vibrations. The experimental spectrum in this range consists of six peaks, seen in the deconvoluted spectrum in Figure 10b. The spectrum with six peaks is more complex than the spectrum from the C_2 molecular conformer. However, the spectra of C_1 molecular conformers show the number of peaks that are consistent with the experimental spectrum. This observation indicates that the transformation of PETN-III to PETN-IV involves a decrease in molecular symmetry from C_2 to C_1. Since this transformation coincides with the formation of parallel lines on the crystal, it seems that this transition is associated with plastic deformation changes.

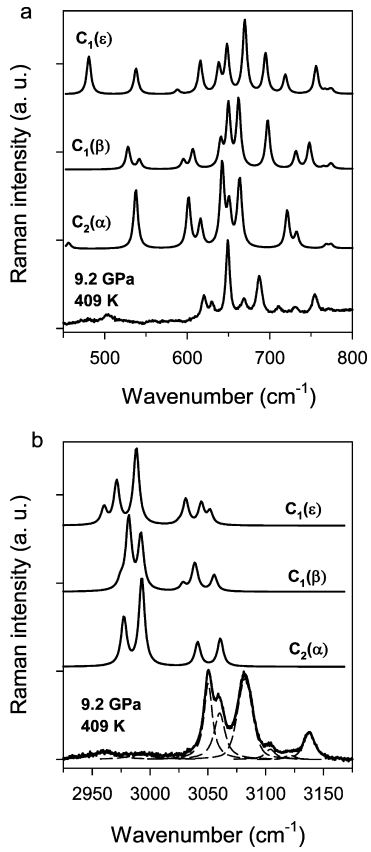

Figure 10. Comparison of Raman spectra at HP–HT with spectra calculated for different molecular conformers of the PETN molecule. The calculated spectra are from ref 8. (a) Spectral region including the CCC deformation modes and (b) spectral region of CH stretching modes; the experimental spectrum is deconvoluted into six peaks.

3.2.3. PETN Phase Diagram. The phase diagram of PETN crystal obtained using argon as a pressure transmitting medium and single crystal samples is presented in Figure 11. Because several aspects of the diagram have been discussed in previous sections, only a comprehensive summary of the results is provided here. The PETN-I to PETN-III transition was observed above ~8.5 GPa at room temperature. For pressures below 8.5 GPa, heated PETN-I remains in the same phase up to the melting/decomposition curve; no transformation to PETN-II was observed. Furthermore, heating the PETN-III at 8.5 GPa did not show a transition back to PETN-I. These results demonstrate that the boundary between PETN-I and PETN-III can be approximated by a vertical line as shown in Figure 11. In other words, the PETN-I to PETN-III transition takes place around 8.5 GPa regardless of temperature.

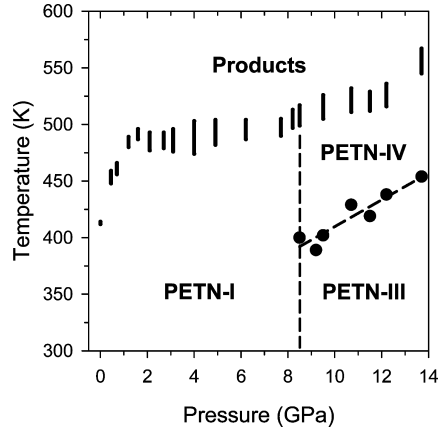

Figure 11. Proposed phase diagram of PETN single crystals in argon pressure medium. Vertical bars denote the onset and completion of melting and/or decomposition, the same as that in Figure 6. The vertical dashed line indicates an approximate transition from PETN-I to PETN-III. Solid circles denote the onset of plastic deformation, seen as the parallel lines on the crystal. The dashed line is the least-squares fit to the experimental data and a boundary line between PETN-III and PETN-IV.

In contrast to PETN-I, which was stable in a large temperature range, PETN-III undergoes a transition to PETN-IV during heating. The phase transition followed plastic deformation changes, which are seen as parallel lines on the crystal surface. Temperature for the PETN-III to PETN-IV transition increased with pressure and is approximated by the dashed line in Figure 11. Further heating of PETN-IV preserves the same phase up to the decomposition temperature. Both PETN-I and PETN-IV either melt or decompose at high temperatures.

The P–T upper bound for melting/decomposition of PETN shows a complex behavior: (i) occurring of melted, decomposed, or both phases in different pressure regions and (ii) nonmonotonic changes of melting/decomposition temperatures with pressure. In particular, the decomposition temper-

dx.doi.org/10.1021/jp404283a | J. Phys. Chem. A 2013, 117, 5306–5313

ature increases significantly in the first 2 GPa, is nearly constant between 2 and 8 GPa, and increases with pressure above ~8 GPa. This increase of decomposition temperature with pressure (above ~8 GPa) indicates that PETN-IV, which only exists at high pressures, is more stable than PETN-I with respect to high-temperature decomposition. The origins of slope changes in the decomposition curve around 8 and 13 GPa are not clear. Nevertheless, they might be related to the change in the decomposition mechanism between PETN-I and PETN-IV (8 GPa) and development of nonhydrostatic stresses (13 GPa). Further work is needed to examine theses conjectures.

Our work has also demonstrated that the PETN response depends strongly on the presence of nonhydrostatic stresses. In particular, the PETN-I to PETN-III transition can occur at a lower mean stress (or pressure) under nonhydrostatic compression. Therefore, we emphasize that boundaries between the PETN phases, presented in Figure 11, may change if nonhydrostatic conditions are present. Using nonhydrostatic medium (glycerol), experiments indicate that the transition onset for PETN-I to PETN-III can be lowered to ~5.3 GPa, consistently with previous studies.[8] However, heating of nonhydrostatically compressed PETN-III converted it back to PETN-I, likely due to the softening of the pressure medium at high temperatures. Therefore, the role of nonhydrostaticity could not be examined on the PETN-III to PETN-IV transition, which occurs at high temperatures. Consequently, it is not clear if this transition could take place under nonhydrostatic conditions.

4. RELEVANCE OF STATIC RESULTS FOR SHOCK COMPRESSION

The static HP–HT results presented here provide further support for the conformational changes proposed to explain the response of shocked PETN single crystals.[6,8,9] In Figure 12, we compare Raman spectra of PETN crystals in the CH stretching region under both shock-wave and static compressions. The shock compression data were obtained for a crystal shocked along the (110) direction to a peak stress of 6.5 GPa, the highest stress for which Raman measurements were obtained.[8] The static compression spectra represent RT measurements under nonhydrostatic compression at 5.3 GPa (Figure 12b) and RT and HT measurements under hydrostatic compression at 9.2 GPa (Figure 12c,d).

In comparing the shock and static spectra, we point out that the shocked spectrum was obtained with a single-pulse laser excitation on a sample prior to decomposition (details regarding the Raman measurements under shock compression can be found elsewhere[9]). Thus, this spectrum has a lower signal-to-background ratio and lower spectral resolution than the static spectra. Furthermore, the shock spectrum was obtained at a different stress than the static spectra. Despite these experimental differences, it is evident that the shock spectrum features are similar to the static compression features at room temperature. In all three cases (plots a, b, and c), a similar pattern of four peaks is observed, suggesting that the high pressure structures under shock and static compressions are very likely the same (PETN-I to PETN-III) and providing good support for the proposed conformation change in PETN shocked along the (110) direction.

We also note that changes under shock compression occur at a stress value, which is close to that for the changes under nonhydrostatic compression. This result is consistent with the fact that shock compression imposes nonhydrostatic conditions

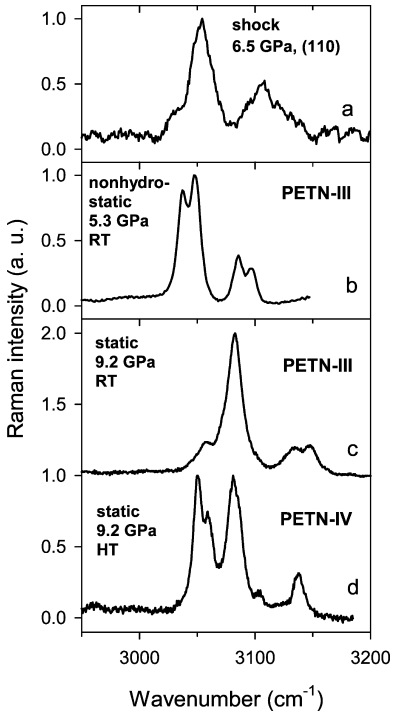

Figure 12. Raman spectra of PETN crystals in the CH stretching range for (a) shock wave compression of (110) oriented crystal to a peak stress of 6.5 GPa (result is taken from ref 8), (b) nonhydrostatic compression to 5.3 GPa at RT, (c) static compression to 9.2 GPa and at RT, and (d) static compression to 9.2 and at HT.

on the crystal due to uniaxial strain loading. Finally, differences between the shock compression spectrum and the PETN-IV spectrum indicate that the PETN-III to PETN-IV transition did not take place under shock compression at least up to 6.5 GPa. Since the shock Raman results are not available above 6.5 GPa, it is not clear if the PETN-III to PETN-IV transition can occur at higher shock stresses.

5. CONCLUSIONS

Raman spectroscopy and optical imaging measurements in a diamond anvil cell were used to examine PETN crystal phases at high pressures and high temperatures to provide insight into the molecular and reactive behavior of PETN at conditions relevant to shock wave induced decomposition. Experiments performed to 14 GPa pressures and temperatures up to 550 K in argon medium demonstrate that the PETN can exist in three phases in this P–T range. The PETN-I to PETN-III transition takes place above ~8.5 GPa and can involve lowering of molecular symmetry from S_4 to C_2. Nonhydrostaticity plays an important role on the pressure onset for this transition. PETN-III transforms to PETN-IV at high temperatures. It is proposed that this transformation involves a further decrease of molecular symmetry from C_2 to C_1. Also, the melting/decomposition curve was found to increase with pressure, indicating that PETN-IV is more stable than PETN-I with respect to high temperatures. Finally, a comparison of static compression results with available shock compression results supports the PETN-I to PETN-III transition proposed under shock compression. This finding underscores the important role of conformational changes on the initiation of shocked PETN crystals, suggested in previous studies

dx.doi.org/10.1021/jp404283a | J. Phys. Chem. A 2013, 117, 5306–5313

AUTHOR INFORMATION

Corresponding Author

*(Z.A.D.) E-mail: dreger@wsu.edu. Phone: 509-335-4233.

Notes

The authors declare no competing financial interest.

ACKNOWLEDGMENTS

Dr. D. E. Hooks from Los Alamos National Laboratory is thanked for providing PETN. This work was supported by the DOE/NNSA Grant #DE-NA0000970.

REFERENCES

(1) Dick, J. J. Effect of Crystal Orientation on Shock Initiation Sensitivity of Pentaerythritol Tetranitrate Explosive. *Appl. Phys. Lett.* **1984**, *44*, 859−861.

(2) Dick, J. J.; Mulford, R. N.; Spencer, W. J.; Pettit, D. R.; Garcia, E.; Shaw, D. C. Shock Response of Pentaerythritol Tetranitrate Single Crystals. *J. Appl. Phys.* **1991**, *70*, 3572−3587.

(3) Dick, J. J.; Ritchie, J. P. Molecular Mechanics Modeling of Shear and the Crystal Orientation Dependence of the Elastic Precursor Shock Strength in Pentaerythritol Tetranitrate. *J. Appl. Phys.* **1994**, *76*, 2726−2737.

(4) Dick, J. J. Anomalous Shock Initiation of Detonation in Pentaerythritol Tetranitrate Crystals. *J. Appl. Phys.* **1997**, *81*, 601−612.

(5) Yoo, C. S.; Holmes, N. C.; Souers, P. C.; Wu, C. J.; Ree, F. H.; Dick, J. J. Anisotropic Shock Sensitivity and Detonation Temperature of Pentaerythritol Tetranitrate Single Crystal. *J. Appl. Phys.* **2000**, *88*, 70−75.

(6) Gruzdkov, Y. A.; Gupta, Y. M. Shock Wave Initiation of Pentaerythritol Tetranitrate Single Crystals: Mechanism of Anisotropic Sensitivity. *J. Phys. Chem. A* **2000**, *104*, 11169−11176.

(7) Dreger, Z. A.; Gruzdkov, Y. A.; Gupta, Y. M.; Dick, J. J. Shock Wave Induced Decomposition Chemistry of Pentaerythritol Tetranitrate Single Crystals: Time-Resolved Emission Spectroscopy. *J. Phys. Chem. B* **2002**, *106*, 247−256.

(8) Hemmi, N.; Dreger, Z. A.; Gruzdkov, Y. A.; Winey, J. M.; Gupta, Y. M. Raman Spectra of Shock Compressed Pentaerythritol Tetranitrate Single Crystals: Anisotropic Response. *J. Phys. Chem. B* **2006**, *110*, 20948−20953.

(9) Gruzdkov, Y. A.; Dreger, Z. A; Gupta, Y. M. Experimental and Theoretical Study of Pentaerythritol Tetranitrate Conformers. *J. Phys. Chem. A* **2004**, *108*, 6216−6221.

(10) Winey, J. M.; Gupta, Y. M. Anisotropic Material Model and Wave Propagation Simulations for Shocked Pentaerythritol Tetranitrate Single Crystals. *J. Appl. Phys.* **2010**, *107*, 103505.

(11) Dreger, Z. A.; Gupta, Y. M. Raman Spectroscopy of High-Pressure−High-Temperature Polymorph of Hexahydro-1,3,5-trinitro-1,3,5-triazine (ε-RDX). *J. Phys. Chem. A* **2010**, *114*, 7038−7047.

(12) Dreger, Z. A.; Gupta, Y. M. Phase Diagram of Hexahydro-1,3,5-trinitro-1,3,5-triazine Crystals at High Pressures and Temperatures. *J. Phys. Chem. A* **2010**, *114*, 8099−8105.

(13) Dreger, Z. A.; Gupta, Y. M. Decomposition of γ-Cyclotrimethylene Trinitramine (γ-RDX): Relevance for Shock Wave Initiation. *J. Phys. Chem. A* **2012**, *116*, 8713−8717.

(14) Dreger, Z. A.; McCluskey, M. D.; Gupta, Y. M. High Pressure−High Temperature Decomposition of γ-Cyclotrimethylene Trinitramine. *J. Phys. Chem. A* **2012**, *116*, 9680−9688.

(15) Booth, A. D.; Llewellyn, F. J. The Crystal Structure of Pentaerythritol Tetranitrate. *J. Chem. Soc.* **1947**, 837−846.

(16) Trotter, J. Bond Lengths and Angles in Pentaerythritol Tetranitrate. *Acta Crystallogr.* **1963**, *16*, 698−699.

(17) Cady, H. H.; Larson, A. C. Pentaerythritol Tetranitrate II: Its Crystal Structure and Transformation to PETN I; an Algorithm for Refinement of Crystal Structures with Poor Data. *Acta Crystallogr.* **1975**, *B31*, 1864−1869.

(18) Lipinska-Kalita, E. K.; Pravica, G. M.; Nicol, M. Raman Scattering Studies of the High-Pressure Stability of Pentaerythritol Tetranitrate, $C(CH_2ONO_2)_4$. *J. Phys. Chem. B* **2005**, *109*, 19223−19227.

(19) Pravica, M.; Lipinska-Kalita, K.; Quine, Z.; Romano, E.; Shen, Y.; Nicol, M. F.; Pravica, W. J. Studies of Phase Transitions in PETN at High Pressures. *J. Phys. Chem. Solids* **2006**, *67*, 2159−2163.

(20) Ciezak, J.; Byrd, E. F. C.; Rice, B. M. Exploring the High-Pressure Behavior of PETN: A Combined Quantum Mechanical and Experimental Study *Proceedings of the 25th Army Science Conference*, Orlando, FL, Nov 27−30, 2006.

(21) Ciezak, A. J.; Jenkins, A. T. New Outlook on the High-Pressure Behavior of Pentaerythritol Tetranitrate. *Army Res. Lab. Tech. Rep.* **2007**, *4238*, 1−15.

(22) Tschauner, O.; Kiefer, B.; Lee, Y.; Pravica, M.; Nicol, M.; Kim, E. Structural Transition of PETN-I to Ferroelastic Orthorhombic Phase PETN-III at Elevated Pressures. *J. Chem. Phys.* **2007**, *127*, 094502−094502−5.

(23) Gruzdkov, Y. A.; Gupta, Y. M. Vibrational Properties and Structure of Pentaerythritol Tetranitrate. *J. Phys. Chem. A* **2001**, *105*, 6197−6202.

(24) Dreger, Z. A.; Trotman, N.; Gupta, Y. M. Unpublished data.